Different relevance of inactivation and F468 residue in the mechanisms of hEag1 channel blockage by astemizole, imipramine and dofetilide

David Gómez-Varela[a,*,1], Constanza Contreras-Jurado[a,1], Simone Furini[a,b],
Rafael García-Ferreiro[a,2], Walter Stühmer[a], Luis A. Pardo[a]

[a] *Max-Planck-Institute of Experimental Medicine, Department of Molecular Biology of Neuronal Signals, Hermann-Rein-Str, 3, 37075 Göttingen, Germany*
[b] *Department of Electronics, Computer Science and Systems, University of Bologna, Viale Risorgimento 2, 40126 Bologna, Italy*

Abstract The relevance of a point mutation at the C-terminal end of the S6 helix (F468) and the introduction of C-type inactivation in the blockage of hEag1 channels by astemizole, imipramine and dofetilide was tested. C-type inactivation decreased block by astemizole and dofetilide but not imipramine, suggesting different binding sites in the channel. F468C mutation increased IC$_{50}$ for astemizole and imipramine but in contrast to HERG channels, only slightly for dofetilide. Together with measurements on recovery of blocking, our observations indicate that the mechanism of hEag1 blockage by each of these drugs is different, and suggest relevant structural differences between hEag1 and HERG channels.
© 2006 Federation of European Biochemical Societies. Published by Elsevier B.V. All rights reserved.

Keywords: Two-electrode voltage clamp; *Xenopus* oocytes; Ether à go-go; Potassium channels; Mutagenesis; Docking

1. Introduction

Two channels of the Ether á go-go family [1] hEag1 and HERG, have been reported as implicated in tumour progression [2]. In contrast to HERG, hEag1 shows unparalleled specificity for tumour tissue [3,4] (except in the CNS) and its inhibition using astemizole or imipramine reduces proliferation of tumour cells [3,5], both ideal features for a potential anticancer target. Unfortunately, all known hEag1 blockers (including imipramine and astemizole, [6–8]) also inhibit HERG, which represents a serious difficulty for dissecting the functions of hEag1 and from a practical point of view (because of HERG-related cardiac adverse effects [9]). Therefore, both the structural determinants responsible for hEag1 blockage by compounds like astemizole and imipramine and the possible differences in hEag1 and HERG blockage processes

will give us new insights for the future synthesis of specific hEag1 blockers.

Previous studies from our group dealt with biophysical details of the blocking mechanism of hEag1 channels by astemizole and imipramine [10]. However, the structural determinants important for these processes are still unknown. In HERG channels, an intact C-type inactivation and a residue at the C-terminal end of the S6 helix (F656) are crucial for the blockage by several compounds [11–17]. The influence of both features in hEag1 blockage by drugs, including astemizole and imipramine is still unknown and was the goal of the present work. We found clear differences in how the effects of the drugs are altered by mutations, and clear indications that at the molecular level the blocking mechanisms for HERG and hEag1 are distinct. Additionally, we performed *in silico* molecular modelling that supports our interpretation of the experimental findings in an independent way.

2. Materials and methods

2.1. Molecular biology

Mutations were introduced into the pSGEM-hEAG1 [18] using the QuikChange XL site-directed mutagenesis kit (Stratagene). All constructs were thereafter sequenced in full. The forward primer used to generate hEag1F468C was (5′–3′; the reverse primer had the complementary sequence): TATGCCACCATCTGCGGGAATGTGACG.

hEag1T432S/A443S was constructed sequentially (first T432S and then A443S). The forward oligonucleotides used were: TCTCCTCG-TTGTATTTCACAATGTCCAGCCTCACC (T432S) and TGGGA-ACATCTCCCCATCCACAGACATTG (A443S).

Oocyte preparation and electrophysiological recordings were performed as described elsewhere [19].

2.2. Data analysis

Curve-fittings were performed using Igor Pro (WaveMetrics). Half-maximal inhibitory drug concentration (IC$_{50}$) values and Hill coefficients (h) were obtained through fittings to the Hill equation. Deactivation kinetics was determined by exponential fitting. Data are represented as means ± S.E.M., where n is the number of oocytes. Statistical significance was considered at $P < 0.01$ in two-tailed Student t test.

2.3. Molecular modelling

Structural models of hEag1 and HERG were generated by homology to the Kv1.2 Protein Data Bank entry 2A79 [20] for the open state. Proteins were aligned with the program T-Coffee (Table 1) [21]. Aligned sequences were submitted to SWISS-MODEL [22] to obtain the protein structures that were replicated in four identical subunits and symmetrically placed around the pore axis to build the tetrameric

*Corresponding author. Fax: +49 551 3899644.
E-mail address: Gomez@em.mpg.de (D. Gómez-Varela).

[1] D.G.V. and C.C.J. are equal contributors.
[2] In the memory of Rafael García Ferreiro.

Table 1
Alignment of hEag1, HERG1 and Kv1.2 channels from the pore helix region to the final residue of the S6 segment

	Pore helix	Filter	Inner helix
hEag1	YISSLYFTMTST	SVGFGNIAPSTI	EKIFAVAIMMIGSLLYATIFGV
HERG1	YVTALYFTFSST	SVGFGNVSPNTS	EKIFSICVMLIGSLMYASIFGV
Kv1.2	IPDAFWWAVVST	TVGYGDMVPTTG	GKIVGSLCAIAGVLTIALPVPI

channels. Finally, channel molecules were energy minimised by 500 steps of steepest descent, using AMBER [23]. Since energy minimisations were performed in the absence of solvent and lipid bilayer, the protein backbone was restrained with a force constant of 7 Kcal mol^{-1} Å^{-2}.

Imipramine, astemizole and dofetilide were modelled in the protonated state. Partial atomic charges of all the drugs were parameterised by the ANTECHAMBER module of AMBER. Protein atomic charges were defined according to the AMBER99 force field.

The docking procedure was performed using AUTODOCK 3.0 [24]. AUTODOCK performs the automated docking of a flexible ligand in a rigid receptor, minimizing an empirical energy function on a 3D grid. All bound angles in the ligands were free to rotate. The grid was defined to cover the whole internal vestibule of the channels and the energy was minimised by Lamarckian genetic algorithm. In order to achieve a broad statistical analysis, every binding position search was carried out by 150 docking runs [25]. The results were clustered according to the root mean square distance (RMSD). Binding positions with a RMSD lower than 2 Å were placed in the same cluster [25]. The binding position with the lowest energy in the group of most populated cluster was selected for the $R_{closest}$ analysis.

2.4. Drugs

Astemizole, N-methyl-astemizole, dofetilide and MK-499, were diluted from a DMSO stock solution. The final concentration of DMSO was always 0.1%, a concentration that showed no effects on hEag1 currents (data not shown). Imipramine was used from stocks in distilled water. Astemizole and imipramine were purchased from Sigma. Pfizer and Merck and Co. kindly supplied Dofetilide and MK-499, respectively.

3. Results and discussion

3.1. Charged astemizole blocks from the intracellular side of hEag1 channels

Our laboratory [10] reported previously that in contrast to imipramine, astemizole blocks a significant amount of hEag1 current from the extracellular side. Although the kinetics of this blockage are compatible with drug equilibration across
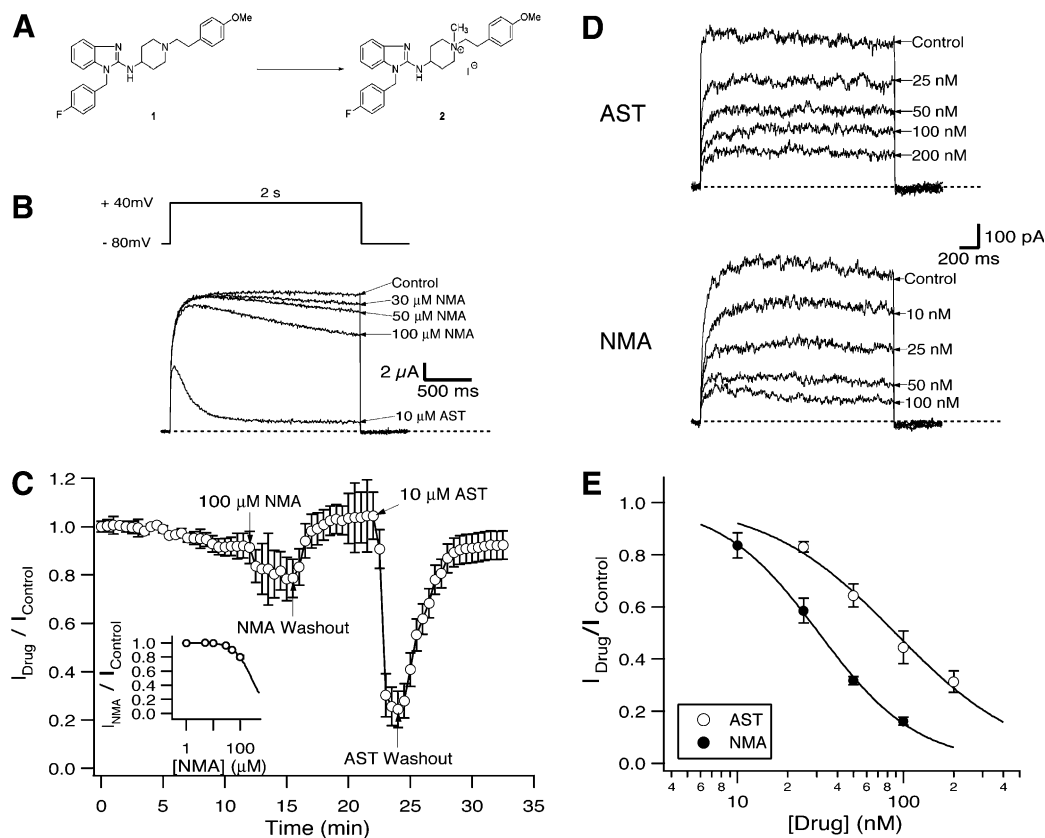

Fig. 1. Characterisation of hEag1 inhibition by NMA. (A) Chemical transformation of AST (1) into the charged derivate NMA (2). (B) hEag1 currents elicited by the depicted voltage protocol applied at 0.05 Hz in the presence of increasing concentrations of NMA or 10 μM AST. The dashed line indicates the zero current level. (C) Time course of normalised current amplitude (n = 4) in the presence of the NMA concentrations indicated in B (for clarity we indicated only the addition of 100 μM NMA), after NMA washout, in the presence of 10 μM AST and after washout. Currents were measured at the end of the pulse at +40 mV and normalised to the amplitude before the addition of the NMA (Control in B). Inset, NMA normalised dose–response curve (n = 10) obtained using the same protocol as described in B. The respective IC$_{50}$ values and Hill coefficients were 262.5 ± 22.5 μM and 1.4 ± 0.1. (D) hEag1 currents in inside-out patches in the presence of increasing concentrations of AST and NMA. Traces obtained using the same protocol as in B. (E) Normalised dose–response curves (n = 4–6). Currents were normalized as in C. Respective IC$_{50}$ values and Hill coefficients were 30 ± 0.7 nM and 1.46 ± 0.05 for NMA, and 91 ± 5.9 nM and 1.11 ± 0.1 for AST.

the membrane [10], the existence of a binding site on the extracellular side of the hEag1 channel protein could not be excluded.

We synthesised the permanently charged, quaternary derivative of astemizole, *N*-methyl-astemizole (NMA; Fig. 1A). Application of 100 μM NMA to the bathing solution reduced current amplitude by ∼20% ($IC_{50} > 100$ μM; Fig. 1B and inset Fig 1C). In contrast, in the same oocyte 10 μM astemizole (AST) blocked ∼90% (Fig. 1B and C).

The lack of NMA effect is not due to loss of affinity for hEag1. NMA applied to the intracellular side of inside-out patches efficiently reduces the current amplitude (Fig. 1D). Together with our previous studies [10], our data demonstrated that both AST and NMA block the channel from the intracellular side and that the charged form of AST (NMA) blocks more effectively (Fig. 1E).

3.2. The effect of the mutations T432S/A443S and F468C on the hEag1 blockage by astemizole (AST)

Intact C-type inactivation seems to be an important requisite for the high-affinity block by methanesulfonanilides in HERG channels [11]. Similarly, introduction of C-type inactivation into bovine Eag channels by a double mutation (T432S/

Table 2
Concentration-dependent block of hEag1 WT, T432S/A443S and F468C by AST, IMI and DOF

	WT	T432S/A443S	F468C
AST	2.8 ± 0.1 ($n = 9$)	1.2 ± 0.1 ($n = 10$)	49.8 ± 2.1 ($n = 7$)
IMI	40.2 ± 0.3 ($n = 10$)	71.5 ± 1.7 ($n = 8$)	202.5 ± 5.9 ($n = 11$)
DOF	29.6 ± 1.1 ($n = 9$)	8.2 ± 0.6 ($n = 10$)	67.7 ± 4.2 ($n = 10$)

IC_{50} values in μM, obtained as in Fig. 2.

A443S) increases the potency of blockage by dofetilide [26]. These mutations in the context of hEag1 produce C-type inactivation (Fig. 2A, T432S/A443S *traces*). Additionally, deactivation of this mutant is slowed at all voltages between −70 and −140 mV, and the voltage-dependence of the activation process is 10–15 mV left-shifted (data not shown).

AST did not affect the activation or inactivation kinetics of this mutant (data not shown), and we therefore determined IC_{50} values by measuring hEag1 current after a steady state blockage was achieved for each AST concentration, either at the end of a +40 mV depolarizing steps for hEag1 wild type (WT) or in the peak at +40 mV for hEag1 T432S/A443S. Under these conditions, the double mutation increased the potency of hEag1 blockage by AST (Table 2 and Fig. 2B).
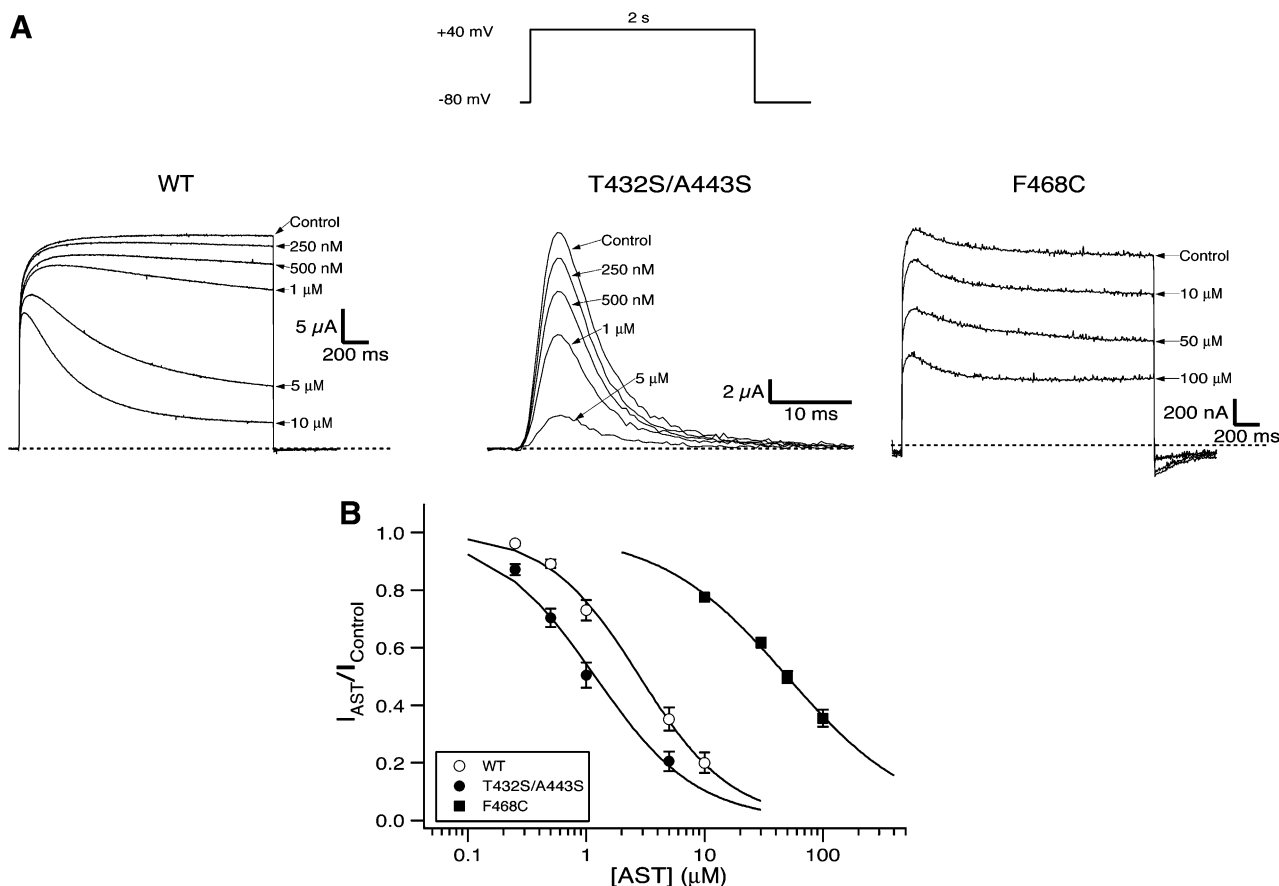

Fig. 2. Concentration-dependent block of hEag1 WT, T432S/A443S and F468C by AST. (A) hEag1 currents elicited by the depicted protocol (0.05 Hz) after steady-state blockage with the indicated AST concentrations for WT, T432S/A443S and F468C. (B) Normalised dose–response curves ($n = 7$–10) obtained from experiments as described in A. Currents were measured at the end of the pulse at +40 mV in WT and F468C and at the peak at +40 mV for T432S/A443S, and normalised to the amplitude of the current prior to the addition of the drugs (Control in A). The respective IC_{50} values and Hill coefficients were 2.8 ± 0.1 μM and 1.11 ± 0.05 for WT, 1.2 ± 0.1 μM and 1 ± 0.07 for T432S/A443S, and 49.8 ± 2.1 μM and 0.8 ± 0.04 for F468C.

It is well documented that Phe 656 in HERG is crucial for the binding of AST [27] and other blockers [16,17,28,29], but the influence of the analogous residue (F468) in hEag1 blockage had not been determined. F468C mutation did not alter the activation or deactivation processes of hEag1 (data not shown), although we cannot definitely discard any alteration of channel kinetics because of the reduced expression levels of the mutant, as reported for a mutation in HERG F656 [30].

hEag1F468C showed an IC_{50} for AST (after reaching steady-state blockage) ~20 times higher than wild type channels (Table 2 and Fig. 2B). This result constitutes the first evidence that F468 plays a crucial role in hEag1 blocking mechanisms, as demonstrated for AST.

3.3. Effects of mutations T432S/A443S and F468C on the hEag1 blockage by imipramine (IMI) and dofetilide (DOF)

AST and IMI compete for the inhibition of hEag1 channels, suggesting that both drugs have an overlapping intracellular binding site [10]. To test this hypothesis, we compared the influence of C-type inactivation and F468C mutation in block by IMI to the results obtained with AST (see above). Table 2 shows that the IC_{50} of IMI for hEag1 WT channels is 10 times higher than that for AST, in good agreement with the differences determined previously in HEK293 cells [10]. Surprisingly, in contrast to astemizole, the introduction of C-type inactivation in hEag1 increased the IC_{50} of IMI rather than reducing it. Although this difference could be due to differences in state-dependence of binding, this result suggests a distinct binding site for each drug. Interestingly, F468C mutation increased IC_{50} suggesting that F468 is an important residue in hEag1 blockage by both IMI and AST.

We extended our study to characterise the hEag1 blocking process by dofetilide. The IC_{50} value obtained for DOF in hEag1 WT channels is in agreement with that previously reported for bovine Eag channels (31.8 μM, Table 2; [26]). The introduction of inactivation increased the potency of blocking by DOF, similarly to bEag [26]. This result suggests that the molecular determinants of DOF blocking are very alike for the human and the bovine Eag1 isoforms. Surprisingly, the IC_{50} value obtained for dofetilide in hEag1 F468C is only 2-fold greater than that for hEag1 WT. This loss of affinity is not as dramatic as that for HERG, where a mutation in F656 increases the IC_{50} of DOF 100-fold [13]. Therefore, although our data suggest that the F468 residue plays a role in DOF binding to hEag1 channels, its importance seems to be less than in HERG channels.
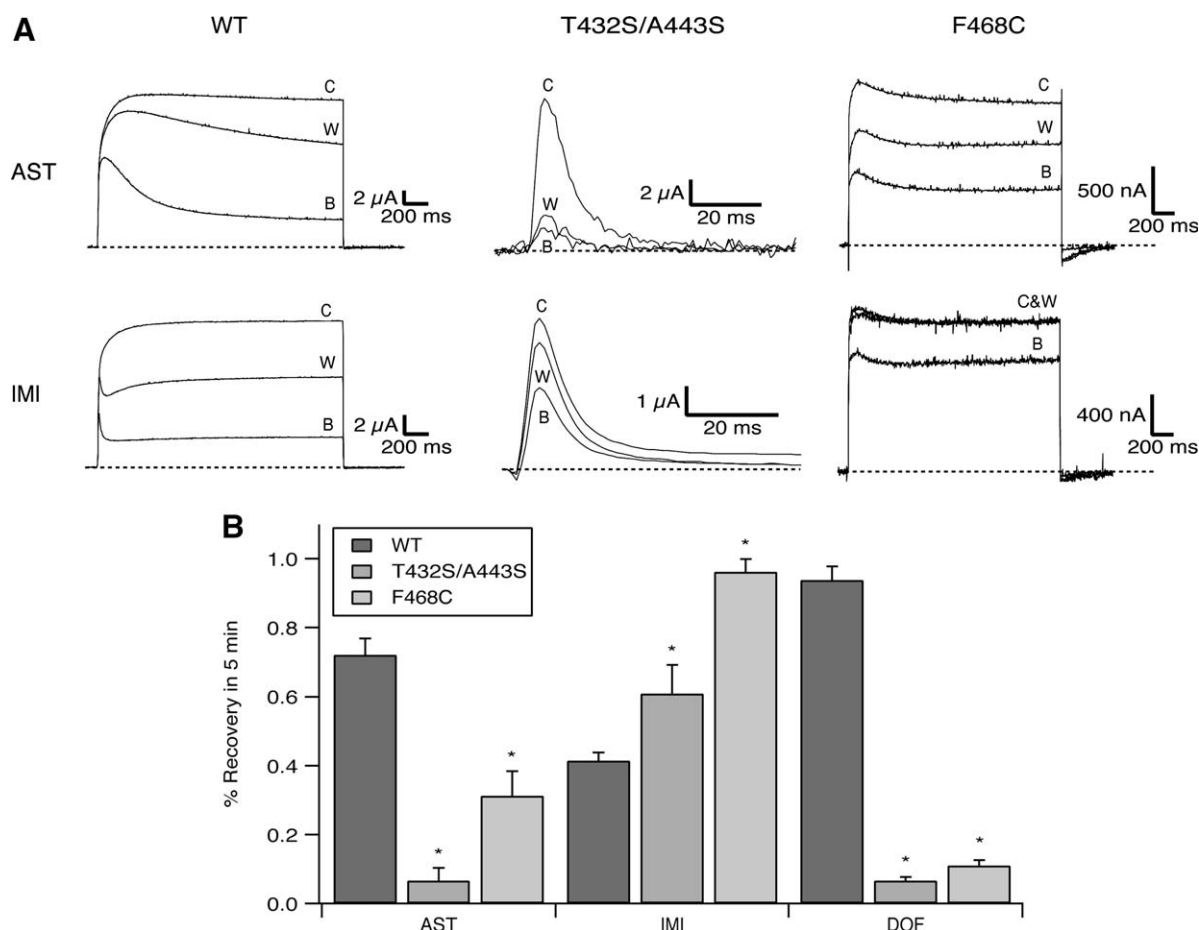

Fig. 3. Differences in AST, IMI and DOF levels of block recovery between hEag1 WT, T432S/A443S and F468C channels. (A) hEag1 WT, T432S/A443S and F468C currents prior to the block (C), after the steady-state block (B) and after the washout (W) of 10 μM AST and 100 μM IMI. Traces were elicited by the same protocol as in Fig. 2. (B) Percentage of recovered current at +40 mV after 5 min washing. The current recovered after 5 min of washing was normalized to the total current blocked by each drug. The recovery percentages of AST, IMI and DOF were 72.1 ± 4.6%, 41.4 ± 2.4% and 93.7 ± 4%, respectively for WT, 6.7 ± 3.7%, 61 ± 8.2% and 6.6 ± 1%, respectively for T432S/A443S, and 31.2 ± 7.2%, 96.2 ± 3.7% and 11 ± 1.5%, respectively for F468C. The bars represent the means ± S.E.M. of 5–8 oocytes.

3.4. Mutations T432S/A443S and F468C alter the recovery from AST-, IMI- and DOF-mediated blockage in different ways

The effects of introduction of C-type inactivation into hEag1 strongly suggest different binding sites for IMI, AST and DOF. We further explored this possibility with studies on the recovery of block.

After blocking hEag1 WT current with either 10 μM AST, 100 μM IMI or 100 μM DOF (Fig. 3A and B), between 40% and 90% recovery was achieved after 5 min wash, strongly

indicating that none of these drugs are trapped in the hEag1 channels during closing. In contrast, T432S/A443S and F468C mutations significantly slowed the recovery from block by AST and DOF, but not by IMI. This is not due to the less efficient IMI-mediated hEag1 inhibition, because we obtained the same results when lower concentrations of AST and DOF were used, sufficient only to block 50% of the T432S/A443S current (data not shown). Similarly, the slower recovery from AST and DOF treatment is probably not due to the low
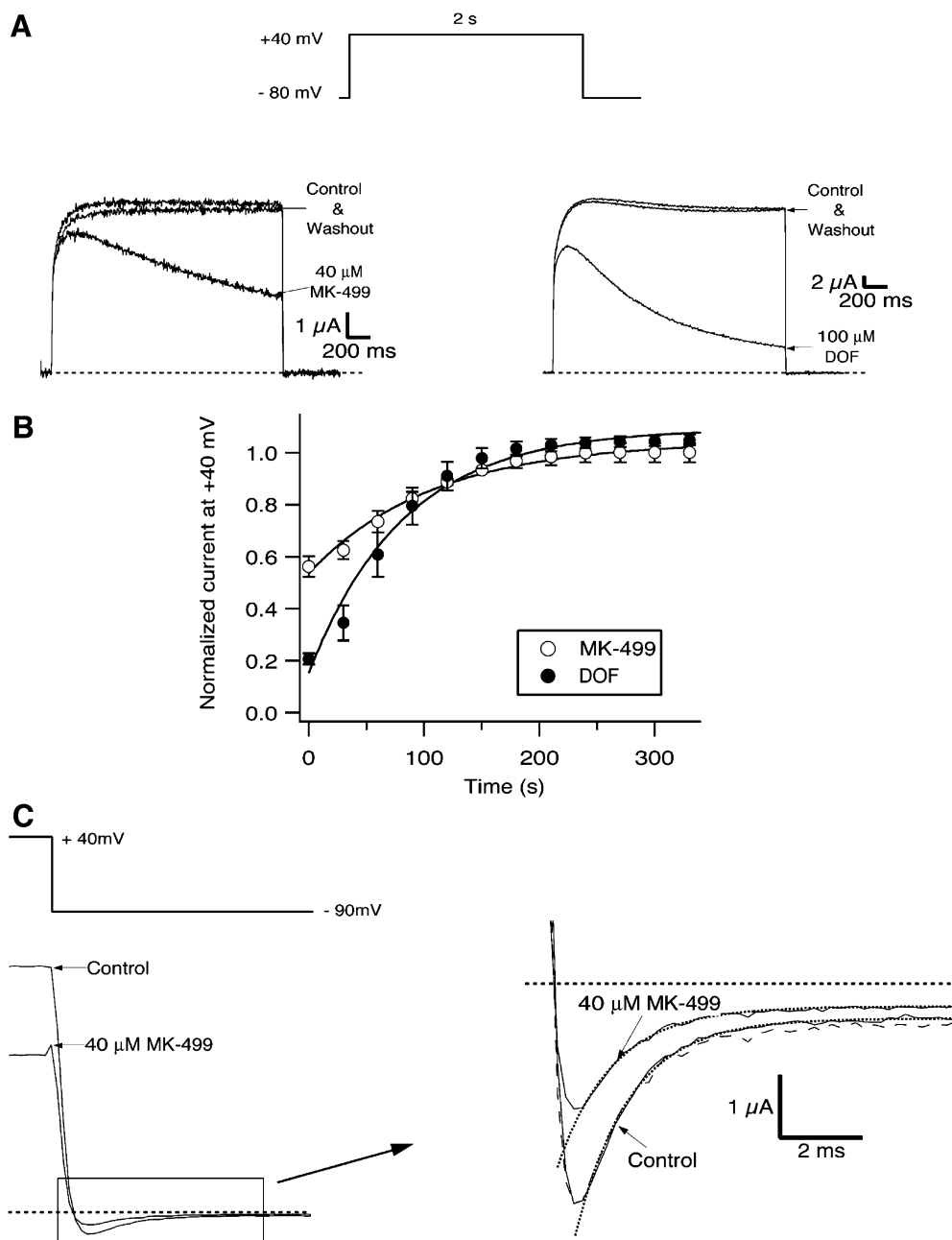

Fig. 4. Mechanisms of block in hEag1 WT channels for DOF and MK-499. (A) hEag1 currents before the block (Control), in the presence of MK-499 (left traces) and DOF (right traces) and after washing (Washout). Traces were produced by the indicated protocol applied at 0.05 Hz. (B) Time-course of the recovery of block during washout of MK-499 and DOF. Currents were measured and normalised as in Fig. 2. (C) hEag1 WT currents in the absence (Control) and presence of MK-499. Traces were produced according to the indicated protocol. The pulse to +40 mV had duration of 2 s. Right panel, tail current traces recorded at − 90 mV, in the absence (Control) and presence of MK-499. The dashed line indicates the zero current level and the dotted line is the scaled tail current after addition of MK-499 to the Control current level, allowing a better comparison of closing kinetics before and after the blocking to be made. Additionally, exponential fits to the currents are shown. The time constants of deactivation are 1.31 ms for Control and 1.26 ms for MK-499.
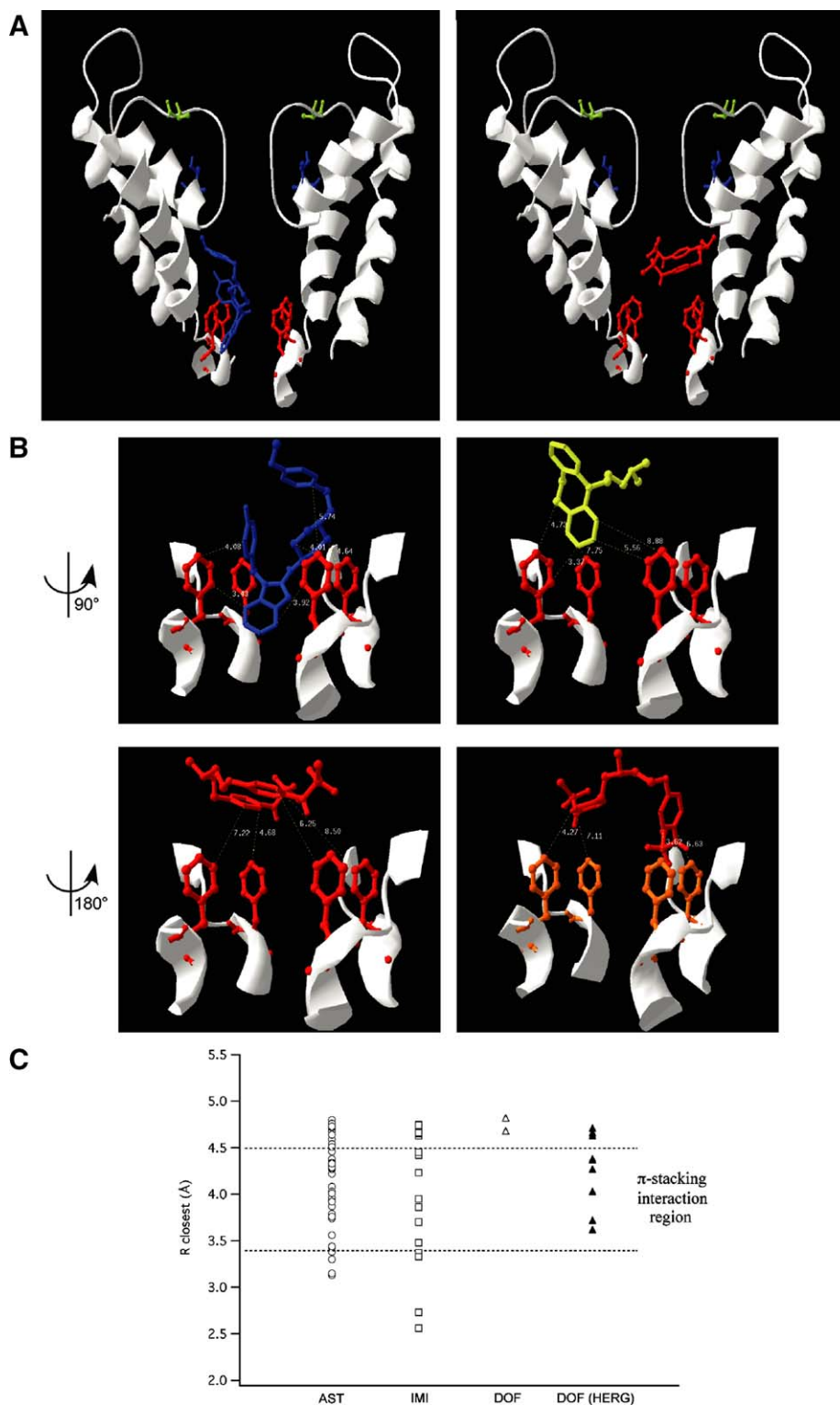
Fig. 5. Docking of AST, IMI and DOF within the cavity of the hEag1 K$^+$ channel as constructed by homology. (A) Homology model showing the S5–S6 domains of two hEag1 subunits with a docked molecule of AST (left panel) and DOF (right panel). F468 (red), T432 (blue) and A443 (yellow) residues are shown as balls and sticks. (B) Close-up stereo views of the C-terminal end of the S6 helix showing the four F468 residues and the relative position of the drugs. The upper panels and lower left panel correspond to hEag1 homology models with AST (blue, upper left), IMI (yellow, upper right) and DOF (red, lower left). For AST and DOF and for better observation, the structures are rotated about the *Y*-axis with respect to the structures in A as indicated on the left hand side of each schematic. The lower right panel is the HERG homology model with DOF and the F656 residues of the four subunits in orange. In all four panels, the closest distances between the aromatic rings atoms of the phenylalanine residues and the drugs are indicated as dashed lines with the values in Å. (C) Aromatic ring (π-stacking) interactions in terms of phenylalanine aromatic ring atoms within the 3.4–4.5 Å of the drug phenyl ring atoms. The inter-atomic distances ($R_{closest}$) close to this interval are indicated for AST-hEag1 docking (empty circles), IMI-hEag1 docking (empty squares), DOF-hEag1 docking (empty triangles) and DOF-HERG docking (full triangles). The dashed lines represent the $R_{closest}$ values of 3.4 and 4.5 Å.

stimulation frequency used during the washing period, because we did not observe any significant increase in the recovery induced by 20 preconditioning pre-pulses of 400 ms to +40 mV (data not shown). Therefore, the differences in the recovery kinetics substantiate our hypothesis that the binding site in hEag1 shared, at least to some degree, by AST and DOF is different from that of IMI.

3.5. Lack of trapping of dofetilide and MK-499 in hEag1 channels

Since in contrast to HERG channels [26,31] DOF does not block hEag1 channels by a trapping mechanism, we tested the blocking mechanism of hEag1 by MK-499, another methanesulfoanilide.

MK-499 blocked hEag1 with an IC_{50} of 43.5 ± 4.7 μM ($n = 4$, data not shown). Recovery was complete in 5 min (Fig. 4A), with a time constant of 106.8 ± 0.7 s, in the same range as for DOF (82.6 ± 0.9 s, Fig. 4B), strongly indicating that block of hEag1 by MK-499 does not involve a drug trapping mechanism. Additionally, a ''foot in the door'' mechanism [17] does not appear to be implicated in the block of hEag1 by MK-499, because the drug does not alter the kinetics of deactivation, as can be deduced from the overlapping normalised tail currents at −90 mV before and after blockage with 40 μM MK-499 (Fig. 4C). Exponential fits to the tail currents (Fig. 4C) gave time constants of deactivation of 1.3 ± 0.14 ms before, and 1.3 ± 0.16 ms after blocking ($n = 4$).

These results strongly indicate that, unlike in HERG channels, both MK-499 and DOF dissociate from hEag1 before it closes, and therefore blockage is not based on trapping of the drug inside the channel during deactivation. Together with the data concerning the different influence of the Phe residues in hEag1 and HERG blockage by dofetilide, our results strongly suggest structural differences between the internal vestibules of both channels.

3.6. Molecular modeling of hEag1-mediated blockage by AST, IMI and DOF

In order to generate a molecular model of hEag1 to test our hypotheses, we used the crystal structure of Kv1.2 channel [20] as a template. It is important to note that Kv1.2 shows a Pro-Val-Pro motif in the S6 domain that has been described to be important for curving the inner helices during channel activation [32], while the hEag1 channel, like KvAP, has a Gly residue in the corresponding position. We reached identical conclusions using either KvAP or Kv1.2 as a template, probably because the Gly residue in KvAP also produces a curvature of the inner helices [20]. In order to dock several open channel blockers, we decided to only comment on our results obtained employing Kv1.2. (open conformation), rather than KvAP (close conformation).

Fig. 5A shows the docking model for AST and DOF in the hEag1 vestibule. At first glance, it is clear that the hydrophobic rings of AST are closer than those of DOF to the Phe residue rings. It is also interesting to note that, although the conformation of the inactivating mutant (T432S/A443S) could not be predicted, our model suggests that the effects observed in the double mutant T432S/A443S could be allosteric, since neither of these two residues are in close proximity to the drugs. Current models predict that C-type inactivation of HERG results in a twisting of the S6 helices and a repositioning of F656, to increase the sensitivity of the channel [33]. Therefore, a similar

movement is possible in the inner helices of hEag1 channels during C-type inactivation, thereby changing the position of some amino acids and increasing the affinity for AST and DOF but not IMI. Further experiments will be necessary to test this possibility. The *in silico* analysis also predicts that other residues in the selectivity filter could interact with the drugs and be important for their stabilization inside the inner vestibule, as described for some residues at the base of the pore helix of HERG and hEag1 [15,34].

Interestingly, molecular modelling also provides a possible explanation for the effects of the F468 mutation. It is accepted that a π–π stacking interaction between two hydrophobic aromatic rings is energetically favourable dependent on the orientation and proximity of the phenyl groups [35,36]. The distance between the carbon atoms of the interacting rings must be between 3.4 and 4.5 Å [35,36]. To predict interactions between the different drugs and the F468 residues, we measured the distances ($R_{closest}$) between the four Phe rings of the channel and the atoms of the aromatic rings of the drugs. Fig. 5C indicates all the $R_{closest}$ values close to this interval for the three different drugs. Only some phenyl groups of AST and IMI but not of DOF show $R_{closest}$ values within the 3.4–4.5 Å interval with respect to phenylalanine hydrophobic rings in the channel. This result gives us a theoretical explanation for the weak effect that the F468 mutation has on the block achieved by DOF and the large effect observed for AST and IMI.

The usefulness of the $R_{closest}$ parameter as an indication for possible π–π stacking interactions was validated by molecular modelling of HERG (Fig. 5B, lower right) and studying the docking of DOF. Interestingly, $R_{closest}$ analysis shows that DOF is closer to the Phe residues in HERG than in hEag1 channels (Fig. 5C). This would agree with recent studies that suggest that the orientation of the S6 aromatic residues with respect to the central cavity of HERG differs from those of Eag channels [33]. Although other interactions must be important for DOF binding to HERG channels, this data could explain why a mutation in these Phe residues affects DOF-mediated block more HERG than to hEag1.

In summary, the experimental differences detected in this study between AST, IMI and DOF blocking processes to hEag1 channels correlate well with information obtained from our molecular modelling approach.

References

[1] Warmke, J., Drysdale, R. and Ganetzky, B. (1991) A distinct potassium channel polypeptide encoded by the Drosophila eag locus. Science 252, 1560–1562.
[2] Pardo, L.A., Contreras-Jurado, C., Zientkowska, M., Alves, F. and Stuhmer, W. (2005) A distinct potassium channel polypeptide encoded by the Drosophila eag locus. J. Membr. Biol. 205, 115–124.
[3] Gavrilova-Ruch, O., Schonherr, K., Gessner, G., Schonherr, R., Klapperstuck, T., Wohlrab, W. and Heinemann, S.H. (2002) Effects of imipramine on ion channels and proliferation of IGR1 melanoma cells. J. Membr. Biol. 188, 137–149.
[4] Ludwig, J., Terlau, H., Wunder, F., Bruggemann, A., Pardo, L.A., Marquardt, A., Stuhmer, W. and Pongs, O. (1994) Functional expression of a rat homologue of the voltage gated either a go-go potassium channel reveals differences in selectivity

and activation kinetics between the Drosophila channel and its mammalian counterpart. Embo J. 13, 4451–4458.

[5] Ouadid-Ahidouch, H., Le Bourhis, X., Roudbaraki, M., Toillon, R.A., Delcourt, P. and Prevarskaya, N. (2001) Changes in the K+ current-density of MCF-7 cells during progression through the cell cycle: possible involvement of a h-ether.a-gogo K+ channel. Receptors Channels 7, 345–356.

[6] Suessbrich, H., Waldegger, S., Lang, F. and Busch, A.E. (1996) Blockade of HERG channels expressed in *Xenopus oocytes* by the histamine receptor antagonists terfenadine and astemizole. FEBS Lett. 385, 77–80.

[7] Zhou, Z., Vorperian, V.R., Gong, Q., Zhang, S. and January, C.T. (1999) Block of HERG potassium channels by the antihistamine astemizole and its metabolites desmethylastemizole and norastemizole. J. Cardiovasc. Electrophysiol. 10, 836–843.

[8] Teschemacher, A.G., Seward, E.P., Hancox, J.C. and Witchel, H.J. (1999) Inhibition of the current of heterologously expressed HERG potassium channels by imipramine and amitriptyline. Br. J. Pharmacol. 128, 479–485.

[9] Sanguinetti, M.C. and Tristani-Firouzi, M. (2006) hERG potassium channels and cardiac arrhythmia. Nature 440, 463–469.

[10] Garcia-Ferreiro, R.E., Kerschensteiner, D., Major, F., Monje, F., Stuhmer, W. and Pardo, L.A. (2004) Mechanism of block of hEag1 K+ channels by imipramine and astemizole. J. Gen. Physiol. 124, 301–317.

[11] Ficker, E., Jarolimek, W., Kiehn, J., Baumann, A. and Brown, A.M. (1998) Molecular determinants of dofetilide block of HERG K+ channels. Circ. Res. 82, 386–395.

[12] Herzberg, I.M., Trudeau, M.C. and Robertson, G.A. (1998) Transfer of rapid inactivation and sensitivity to the class III antiarrhytmic drug E-4031 from HERG to M-eag channels. J. Physiol. 511, 3–14.

[13] Lees-Miller, J.P., Duan, Y., Teng, G.Q. and Duff, H.J. (2000) Molecular determinant of high-affinity dofetilide binding to HERG1 expressed in *Xenopus oocytes*: involvement of S6 sites. Mol. Pharmacol. 57, 367–374.

[14] Wang, S., Morales, M.J., Liu, S., Strauss, H.C. and Rasmusson, R.L. (1997) Modulation of HERG affinity for E-4031 by [K+]o and C-type inactivation. FEBS Lett. 417, 43–47.

[15] Mitcheson, J.S., Chen, J., Lin, M., Culberson, C. and Sanguinetti, M.C. (2000) A structural basis for drug-induced long QT syndrome. Proc. Natl. Acad. Sci. USA 97, 12329–12333.

[16] Sanchez-Chapula, J.A., Navarro-Polanco, R.A., Culberson, C., Chen, J. and Sanguinetti, M.C. (2002) Molecular determinants of voltage-dependent human ether-a-go-go related gene (HERG) K+ channel block. J. Biol. Chem. 277, 23587–23595.

[17] Kamiya, K., Mitcheson, J.S., Yasui, K., Kodama, I. and Sanguinetti, M.C. (2001) Open channel block of HERG K(+) channels by vesnarinone. Mol. Pharmacol. 60, 244–253.

[18] Pardo, L.A., del Camino, D., Sanchez, A., Alves, F., Bruggemann, A., Beckh, S. and Stuhmer, W. (1999) Oncogenic potential of EAG K(+) channels. Embo J. 18, 5540–5547.

[19] Stuhmer, W. (1992) Electrophysiological recording from *Xenopus oocytes*. Methods Enzymol. 207, 319–339.

[20] Long, S.B., Campbell, E.B. and Mackinnon, R. (2005) Crystal structure of a mammalian voltage-dependent Shaker family K+ channel. Science 309, 897–903.

[21] Notredame, C., Higgins, D.G. and Heringa, J. (2000) T-Coffee: A novel method for fast and accurate multiple sequence alignment. J. Mol. Biol. 302, 205–217.

[22] Schwede, T., Kopp, J., Guex, N. and Peitsch, M.C. (2003) SWISS-MODEL: An automated protein homology-modeling server. Nucleic Acids Res. 31, 3381–3385.

[23] Case, D. et al. (2004) AMBER 8, University of California, San Francisco.

[24] Morris, G.M., Goodsell, D.S., Halliday, R.S., Huey, R., Hart, W.E., Belew, R.K. and Olson, A. (1998) Automated docking using a Lamarckian genetic algorithm and empirical binding free energy function. J. Computat. Chem. 19, 1639.

[25] Hetenyi, C. and van der Spoel, D. (2002) Efficient docking of peptides to proteins without prior knowledge of the binding site. Protein Sci. 11, 1729–1737.

[26] Ficker, E., Jarolimek, W. and Brown, A.M. (2001) Molecular determinants of inactivation and dofetilide block in ether a-go-go (EAG) channels and EAG-related K(+) channels. Mol. Pharmacol. 60, 1343–1348.

[27] Ficker, E., Obejero-Paz, C.A., Zhao, S. and Brown, A.M. (2002) The binding site for channel blockers that rescue misprocessed human long QT syndrome type 2 ether-a-gogo-related gene (HERG) mutations. J. Biol. Chem. 277, 4989–4998.

[28] Mitcheson, J.S., Chen, J., Lin, M., Culberson, C. and Sanguinetti, M.C. (2000) A structural basis for drug-induced long QT syndrome. Proc. Natl. Acad. Sci. USA, 97, 12329–12333.

[29] Ridley, J.M., Milnes, J.T., Duncan, R.S., McPate, M.J., James, A.F., Witchel, H.J. and Hancox, J.C. (2006) Inhibition of the HERG K+ channel by the antifungal drug ketoconazole depends on channel gating and involves the S6 residue F656. FEBS Lett. 580, 1999–2005.

[30] Fernandez, D., Ghanta, A., Kauffman, G.W. and Sanguinetti, M.C. (2004) Physicochemical features of the HERG channel drug binding site. J. Biol. Chem. 279, 10120–10127.

[31] Carmeliet, E. (1992) Voltage- and time-dependent block of the delayed K+ current in cardiac myocytes by dofetilide. J. Pharmacol. Exp. Ther. 262, 809–817.

[32] del Camino, D., Holmgren, M., Liu, Y. and Yellen, G. (2000) Blocker protection in the pore of a voltage-gated K+ channel and its structural implications. Nature 403, 321–325.

[33] Chen, J., Seebohm, G. and Sanguinetti, M.C. (2002) Position of aromatic residues in the S6 domain, not inactivation, dictates cisapride sensitivity of HERG and eag potassium channels. Proc. Natl. Acad. Sci. USA 99, 12461–12466.

[34] Gessner, G., Zacharias, M., Bechstedt, S., Schonherr, R. and Heinemann, S.H. (2004) Molecular determinants for high-affinity block of human EAG potassium channels by antiarrhythmic agents. Mol. Pharmacol. 65, 1120–1129.

[35] Hunter, C.A., Singh, J. and Thornton, J.M. (1991) Pi–pi interactions: the geometry and energetics of phenylalanine–phenylalanine interactions in proteins. J. Mol. Biol. 218, 837–846.

[36] McGaughey, G.B., Gagne, M. and Rappe, A.K. (1998) pi-Stacking interactions. Alive and well in proteins. J. Biol. Chem. 273, 15458–15463.